https://doi.org/10.5194/hess-2021-588
Preprint. Discussion started: 30 November 2021

Hydrology and Earth System Sciences
Discussions
Open Access
EGU

Experimental study of non-Darcian flow characteristics in permeable stones

Zhongxia Li[1], Junwei Wan[1], Tao Xiong[1], Hongbin Zhan[2]*, Linqing He[3], Kun Huang[1]*

[1]School of Environmental Studies, China University of Geosciences, 430074 Wuhan, China.

[2]Department of Geology and Geophysics, Texas A & M University, College Station, TX 77843-3115, USA.

[3]Changjiang Institute of Survey Technical Research MWR, Wuhan, China.

* Corresponding authors:

Dr. Hongbin Zhan (zhan@geos.tamu.edu);

Dr. Kun Huang (cugdr_huang@cug.edu.cn).

https://doi.org/10.5194/hess-2021-588
Preprint. Discussion started: 30 November 2021


Hydrology and Earth System Sciences
Discussions

Abstract

This study provides experimental evidence of Forchheimer flow and transition between different flow regimes from the perspective of pore size of permeable stone. We have firstly carried out the seepage experiments of permeable stones with four different mesh sizes, including 24 mesh size, 46 mesh size, 60 mesh size, and 80 mesh size, which corresponding to mean particle sizes (50% by weight) of 0.71 mm, 0.36 mm, 0.25 mm, and 0.18 mm. The seepage experiments show that obvious deviation from Darcian flow regime is visible. In addition, the critical specific discharge corresponding to the transition of flow regimes (from pre-Darcian to post-Darcian) increases with the increase of particle sizes. When the "pseudo" hydraulic conductivity (K) (which is computed by the ratio of specific discharge and the hydraulic gradient) increases with the increase of specific discharge (q), the flow regime is denoted as the pre-Darcian flow. After the specific discharge increases to a certain value, the "pseudo" hydraulic conductivity begins to decrease, and this regime is called the post-Darcian flow. In addition, we use the mercury injection experiment to measure the pore size distribution of four permeable stones with different particle sizes, and the mercury injection curve is divided into three stages. The beginning and end segments of the mercury injection curve are very gentle with relatively small slopes, while the intermediate mercury injection curve is steep, indicating that the pore size in permeable stones is relatively uniform. The porosity decreases as the mean particle sizes increases, and the mean pore size can faithfully reflect the influence of particle diameter, sorting degree and arrangement mode of porous medium on seepage parameters. This study shows that the size of pores is an essential factor for determining the flow regimes. In addition, the Forchheimer coefficients are also discussed in which the coefficient A (which is related to the linear term of the Forchheimer equation) is linearly related to $1/d^2$ as $A = 0.0025\left(1/d^2\right) + 0.003$; while the coefficient B (which is related to the quadratic term of the Forchheimer equation) is a quadratic function of $1/d$ as

https://doi.org/10.5194/hess-2021-588
Preprint. Discussion started: 30 November 2021


Hydrology and Earth System Sciences
Discussions

$B = 1.14\text{E-}06(1/d)^2 - 1.26\text{E-}06(1/d)$. The porosity ($n$) can be used to reveal the effect of sorting degree and arrangement on seepage coefficient. The larger porosity leads to smaller coefficients A and B under the condition of the same particle size.

***Keywords*:** permeable stone, mercury injection experiment, pore size, flow regime, non-Darcian flow.

1. Introduction

Darcy (1857) conducted a steady-state flow experiment in porous media and concluded that the specific discharge was proportional to the hydraulic gradient, which is the Darcy's law described as follow:

$$q = KJ \tag{1-1}$$

where q is the specific discharge, J is the hydraulic gradient, and K is the hydraulic conductivity. However, when the specific discharge increases above a certain threshold, deviation from Darcy's law is evident and the flow regime changes from Darcian flow regime to the so called non-Darcian flow regime (Bear, 1972), which was first observed by Forchheimer (1901), who proposed a widely used non-Darcian flow equation (the Forchheimer equation) as follow:

$$J = Aq + Bq^2 \tag{1-2}$$

where A and B are constants related to fluid properties and pore structure. The first and second terms on the right side of Eq. (1-2) roughly reflect the contributions of viscous and inertial forces (or resistance to flow), respectively.

From the Forchheimer equation, we can see that when the specific discharge is sufficiently small, the inertial force can be ignored, and the equation is transformed to the

https://doi.org/10.5194/hess-2021-588
Preprint. Discussion started: 30 November 2021


Hydrology and Earth System Sciences
Discussions

form of Darcy's law. On the other hand, when the specific discharge is sufficiently large, the viscous force can be ignored, and the equation is transformed to the fully developed turbulent flow.

In addition to the polynomial function such as the Forchheimer equation, there are also several power-law functions proposed to describe the non-Darcian flow, and one of the most commonly used power-law equations is the Izbash equation (Izbash, 1931), which is written as:

$$J = aq^b \tag{1-3}$$

where a and b are the empirical parameters that depend on flow and materials properties, and the coefficient b is usually between 1 and 2.

Because of its applicability for a wide range of velocity spectrum and its sound physics, many scholars have adopted the Forchheimer equation (among many different types of equations) to explore the non-Darcian flow. Besides, the theoretical background of the Forchheimer equation has been discussed in details (Panfilov and Fourar, 2006). Numerous experimental data have confirmed the validity of the Forchheimer equation for a variety of nonlinear flow phenomena (Geertsma, 1974; Scheidegger, 1957; Wright, 1968). The quadratic Forchheimer law has also been revealed as a result of numerical modelling by simulating the Navier–Stokes flow in corrugated channels (Koch and Ladd, 1996; Skjetne et al., 1999; Souto and Moyne, 1997). To sum up, the Forchheimer equation will be selected as a representative to describe non-Darcy flow in this study.

Since the transition between Darcian flow and non-Darcian flow is important and difficult to quantify, different scholars have carried out experiments using a wide range of porous media, including homogeneous and heterogeneous porous media. Most of the experimental studies have focused on the influence of mean particle size on flow state

https://doi.org/10.5194/hess-2021-588
Preprint. Discussion started: 30 November 2021


Hydrology and Earth System Sciences
Discussions

transition using homogeneous porous media. In fact, it was believed that the nonlinear (or non-Darcian) flow behavior in porous media was due to turbulent effect of flow in earlier studies and the Reynold number (*Re*) was widely used to quantify the initiation of non-Darcian flow. Bear (1972) concluded that the critical *Re* (denoted as Re_c) of flow states (or the *Re* value at which flow starts to change from Darcian flow regime to non-Darcian flow regime) is between 1 to 10. This finding was based on experimental data collected in packed sand beds (Ergun, 1952; Fancher and Lewis, 1933; Lindquist, 1933; Scheidegger, 1960). Schneebeli (1955) and Wright (1968) experimentally measured the value of *Re* at the beginning of turbulence and concluded that at very high velocities, the deviation from Darcy's law is due to inertial effects followed by turbulent effects. In addition, Dudgeon (1966) confirmed that Re_c is about 60~150 for relatively coarse particle medium including river gravels, crushed rock particles and glass marbles with grain sizes from 16 mm to 152 mm. Dudgeon (1966) indicated that the deviation from Darcy's law was not entirely due to turbulence, but in a large extent due to inertial forces. Besides, Geertsma (1974) proposed an empirical relationship among the inertial coefficient, permeability and porosity by conducting non-Darcian flow experiments in unconsolidated and consolidated sands. The laser anemometry and flow visualization studies of fluid flow in porous structures were used by Dybbs and Edwards (1984), and they observed the nonlinear behavior at Reynolds numbers around 150. Latifi et al. (1989) found that the transition from unsteady-state laminar flow to non-Darcian flow in packed beds of spheres was between *Re* values of 110 and 370. Seguin et al. (1998) investigated the characterization of flow regimes in various porous media with electrochemical techniques and found that the end of the Darcian flow regime in packed beds of particles appeared at *Re* about 180. Besides, Bu et al. (2014) indicated that the Darcian flow in the packed beds would end at *Re* around 100 by using electrochemical techniques. Sedghi-Asl et al. (2014) found that the Darcy's law was usually not valid for rounded particle

https://doi.org/10.5194/hess-2021-588
Preprint. Discussion started: 30 November 2021


Hydrology and Earth System Sciences
Discussions

sizes greater than 2.8 mm, according to the experimental results of flow in different sizes of rounded aggregates. Our previous experimental research (Li et al., 2017) indicated that when the particle size was smaller than 2.8 mm, the flow state gradually changed from pre-Darcy flow to post-Darcy flow when the specific discharge increased. When the medium particle sizes get even larger, such as 4.5 mm, 6.39 mm, 12.84 mm, and 16 mm (Moutsopoulos et al., 2009), only the post-Darcy flow exists. Based on above analysis, we can see that many previous experiments were carried out on homogeneous porous media, and the non-Darcy flow characteristics are quite different in porous media with various particle sizes.

Among the numerous experimental studies on this issue, it is evident that most of them focused on the effect of the mean particle size rather than the particle size distribution. Recently, a few investigators recognized the importance of particle size heterogeneity in understanding the transition of flow regimes, and have carried out a series of experiments to address the issue. For instance, Van Lopik et al. (2017) provided new experimental data on nonlinear flow behavior in various uniformly graded granular material for 20 samples, ranging from medium sands (d_{50} > 0.39 mm) to gravel (d_{50} >6.34 mm). In addition, they investigated the nonlinear flow behavior through packed beds of 5 different types of natural sand and gravel from unconsolidated aquifers, as well as 13 different composite mixtures of uniformly graded filter sands at different grain size distributions and porosity values (Van Lopik et al., 2019). We have also discussed the effect of particle size distribution on Forchheimer flow and transition of flow regimes in a previous study (Li et al., 2019). And our study showed that the uniformity coefficient of porous media (a term used to describe the pore size distribution) is a critical factor for determining the flow regimes besides the mean particle sizes. Yang et al. (2019) investigated the effects of the particle size distribution on the seepage behavior of a sand particle mixture subjected and evaluated the validity of empirical formulas of permeability and inertia factor used in engineering practice. Shi et al. (2020)

https://doi.org/10.5194/hess-2021-588
Preprint. Discussion started: 30 November 2021


Hydrology and Earth System Sciences
Discussions

discussed the non-Darcy flow behavior of granular limestone with a wide range of porosity from 0.242 to 0.449. Based on the experimental data, Shi et al. (2020) proposed an empirical hydraulic conductivity-porosity relation as well as an expression of inertial coefficient. Regardless of the media investigated are homogeneous or heterogeneous, the essence of the water passing capacity of porous media is pore sizes. Thus, exploring the distribution of pores in porous media is the basis of studying flow dynamics of Darcian and non-Darcian flows.

The purpose of this study is to provide a quantitative analysis on the effects of pore size on the transition of flow regimes between Darcian and non-Darcian flows based on a series of laboratory experiments. To meet the objectives, we have firstly carried out the seepage experiments of permeable stones with four different particle sizes. After that, we have conducted mercury injection experiments on permeable stones with four different particle sizes, and the pore size distributions with different particle sizes are obtained. Finally, the effect of pore size on the transition of flow regimes and Forchheimer coefficients are discussed based on the experimental results.

2. Experimental methodology

2.1 Experimental setup and methods

The experimental device is mainly composed of three parts: a water supply device, a seepage experimental device and a measuring device. The schematic diagram of the experimental apparatus is shown in Fig. 1. The water supply device consists of a tank, a centrifugal pump and a flow regulating valve. The seepage experimental device consists of a permeable stone and a plexiglass column. The measurement device monitors the real-time water temperature and pressure. The water temperature is measured using a thermometer with a precision of measurement of 0.1 °C. The water-level fluctuation is measured to calculate the flow rate by a pressure transducer (CY201, Chengdu test LLC, China) in the range of 0–20 kPa with ±0.1% accuracy. The measuring device consists of a cylindrical tank and a pressure

https://doi.org/10.5194/hess-2021-588
Preprint. Discussion started: 30 November 2021

transducer. The sample of permeable stone is 60 mm in length with a circular cross section of 51.3 mm in diameter. Two pressure transducers are set at the entrance and exit of the column to measure the pressure drop. To minimize the boundary effects, the pressure transducer is placed 30 mm away from either end of the column, and the way of pressure measurement is consistent with our previous studies (Li et al., 2017; Li et al., 2019).

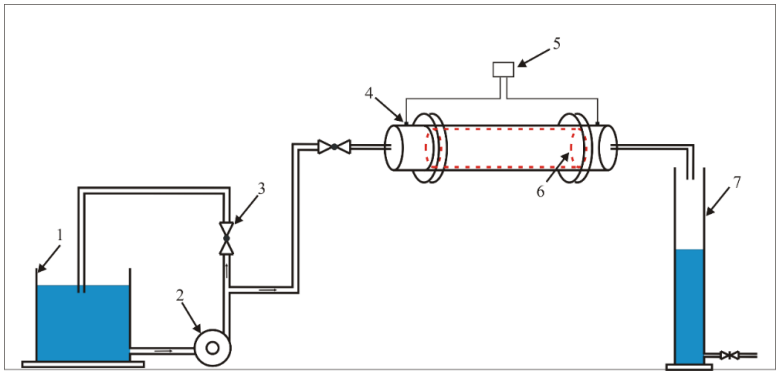

1) tank, 2) Pump, 3) Valve, 4) Pressure sensor, 5) Data collector, 6) Permeable stones, 7) Measurement tank.

Fig. 1 The schematic diagram of experimental apparatus.

2.2 Experimental Materials and Procedures

Four different particle sizes of permeable stones are selected to carry out the seepage experiment in this study. It is necessary to make a brief overview of the preparation process of permeable stone, which is a type of artificially made tight porous medium formed by sand grains and cementing compound. In the process of preparing permeable stone, a certain particle size of sand and cementing compound is put in a mold, and is consolidated at room temperature. We have carried out the seepage experiments of permeable stones with four different mesh sizes, including 24 mesh size, 46 mesh size, 60 mesh size, and 80 mesh size, and the mesh size is defined as the number of mesh elements (all in square shapes) in a one inch by one inch square, thus a greater number of mesh size implies a smaller particle size.

https://doi.org/10.5194/hess-2021-588
Preprint. Discussion started: 30 November 2021

For instance, we can convert above four different mesh sizes of permeable stones into corresponding particle sizes of 0.71 mm, 0.36 mm, 0.25 mm and 0.18 mm, respectively. The pore structure of permeable rock will not change in the process of the seepage experiment under room temperature, and the physical diagrams of four kinds of permeable stones with different particle sizes are shown in Fig. 2 and Fig. 3.

Fig. 2 Physical drawing of permeable stones with four different particle sizes.

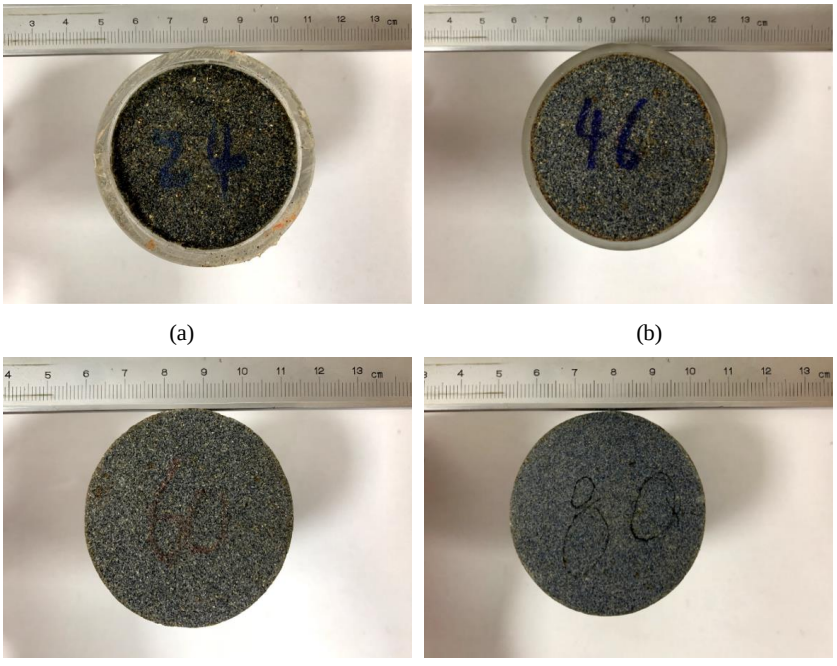

(a) (b)

(c) (d)

Fig. 3 Permeable stones with different particle sizes: (a) 24 mesh size or 0.71 mm, (b) 46 mesh size or 0.36 mm, (c) 60 mesh size or 0.25 mm, and (d) 80 mesh size or 0.18 mm.

https://doi.org/10.5194/hess-2021-588
Preprint. Discussion started: 30 November 2021


Hydrology and Earth System Sciences
Discussions

196 It is worth mentioning that the contact surface of the sample and the plexiglass column
197 is sealed to prevent any preferential flow through the wall of the plexiglass column. After the
198 permeable stone is inserted into the plexiglass column, both ends are sealed with silicone glue.
199 The water passing through the permeable stone is then collected by a cylindrical tank.
200 Moreover, the ratio of the internal diameter of the column to the particle size of permeable
201 stone is greater than 12, which can eliminate any possible wall effect on the seepage
202 according to Beavers et al. (1972). When carrying out the experiment, it usually takes about
203 two hours to saturate the permeable stone. For each packed sample, more than 25 tests with
204 different constant inlet pressures were conducted under steady-state flow condition. In
205 addition, for each group of permeable stone, repeated tests under the same experimental
206 condition were carried out 3-4 times to ensure the accuracy of the results.

207 **3. Results and discussion**

208 **3.1 Permeable stone seepage experiment**

209 In this study, we selected permeable stone with four different particle sizes as the
210 research objects, including 24 mesh size, 46 mesh size, 60 mesh size and 80 mesh size. The
211 mesh size is the number of holes per inch of screen mesh and the particle size is inversely
212 proportional to the mesh size. The mean particle sizes corresponding to the four different
213 mesh sizes are 0.71 mm, 0.36 mm, 0.25 mm, and 0.18 mm, respectively, where the mean
214 particle size is corresponding to 50% by weight hereinafter in this study. Such a definition of
215 mean particle size may be different from some other studies such as Fetter (2001) which has
216 used 10% by weight as the mean particle size. The relationship between the specific
217 discharge (q) and the hydraulic gradient (J) of permeable stones is plotted in Fig. 4. The units
218 of specific discharge mentioned in this study are all converted to meters per day (m/d).

219

https://doi.org/10.5194/hess-2021-588
Preprint. Discussion started: 30 November 2021

Hydrology and Earth System Sciences
Discussions

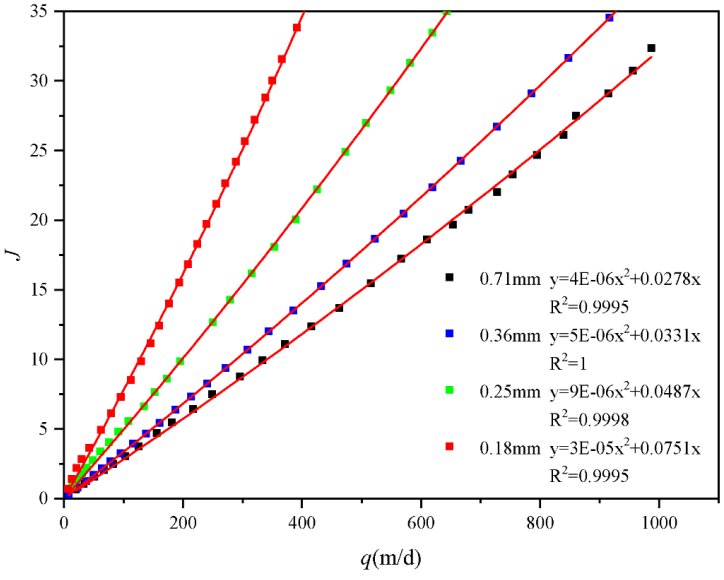

Fig. 4 Variation of J with q of four permeable stones with different particle sizes.

Fig. 4 shows that when q is somewhat the same, a larger mesh size (which means a smaller particle size) will lead to a larger J. And the results are consistent with our previous studies (Huang et al., 2013; Li et al., 2017; Li et al., 2019). However, the nonlinear characteristics of q-J curve are not obvious due to the relatively small velocity range used in the experiments. Nevertheless, the best-fitting results using the Forchheimer equation are satisfactory. To analyze the influence of pore size on seepage flow regimes, we have obtained the relationship between q and the "pseudo" hydraulic conductivity (K) (which is computed using q/J) of four permeable stones with different particle sizes, as shown in Fig. 5. We should point out that the "pseudo" hydraulic conductivity term discussed here for non-Darcian flow is usually not a constant, thus it is different from the hydraulic conductivity term used in Darcy's law, which is a constant. It is obvious that the hydraulic conductivity is not a constant with the increase of specific discharge, so it is called the "pseudo" hydraulic conductivity (Li et al., 2019).

https://doi.org/10.5194/hess-2021-588
Preprint. Discussion started: 30 November 2021

Hydrology and Earth System Sciences
Discussions

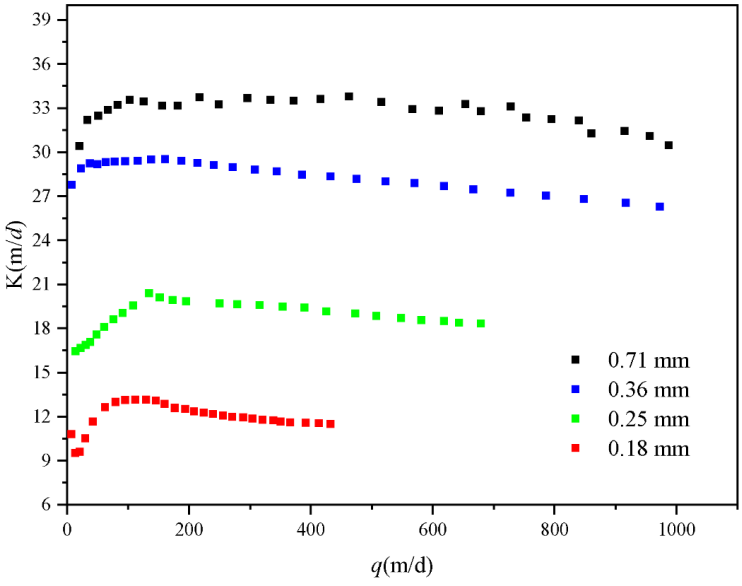

235

236 Fig. 5 Variation of K with q of four permeable stones with different particle sizes.

237 We can divide the q-K curve into two segments: for the first segment, K increases with
238 the increase of q, which is denoted as the pre-Darcian flow. For the second segment, after q
239 increases to a certain value, K begins to decrease with q, which is called the post-Darcian
240 flow. When the hydraulic gradient is small (and q is small as well), a great portion of water is
241 bounded (or becomes immobile) on the surface of solids due to the solid-liquid interfacial
242 force, and only a small fraction of the water is mobile and free to flow through the pores. As
243 the hydraulic gradient increases (and q increases as well), the initial threshold for mobilizing
244 the previously immobile water near the solid-liquid surface is overcome and more water
245 participates in the flow. For this reason, the "pseudo" hydraulic conductivity increases with
246 the increase of hydraulic gradient and the specific discharge in the first segment. When the
247 specific discharge increases to the critical specific discharge (q_c), the "pseudo" hydraulic
248 conductivity is maximized. According to $K=\frac{q}{Aq+Bq^2}=\frac{1}{A+Bq}$ based on Eq. (1-2), we can
249 find that the "pseudo" hydraulic conductivity begins to decrease as the specific discharge

https://doi.org/10.5194/hess-2021-588
Preprint. Discussion started: 30 November 2021


Hydrology and Earth System Sciences
Discussions

continues to increase. Besides, the critical specific discharge corresponding to the transition of flow regimes (from pre-Darcian to post-Darcian) increases with the increase of particle sizes (or decrease of mesh sizes).

3.2 Mercury injection experiment

The particle size, different grain size distributions and degree of sorting are the main factors that determine the size and shape of pores. And the shape of the pores determines the tortuosity and distribution of flow paths, which are related to viscous and inertial flow resistances. It is generally accepted in previous studies that the pore sizes of porous media have an impact on the seepage law (Maalal et al., 2021; Zhou et al., 2019). However, the structure of natural porous media is very complex, and it is difficult to quantify the effects of the arrangement of particles on the seepage law. The characteristics of pore size distribution contains critical information for quantifying the flow regimes. The mercury intrusion porosimetry and the nitrogen adsorption isotherm are two commonly used methods to characterize the pore sizes and their distribution (Rijfkogel et al., 2019). Besides, other techniques can also be used to derive the pore size distribution, such as small-angle neutron and X-ray scattering measurements, CT images and nuclear magnetic resonance (Anovitz and Cole, 2015; Hall et al., 1986; Kate and Gokhale, 2006; Lindquist et al., 2000). In this study we will use the mercury injection experiment to measure the pore size distribution of the four permeable stones with different particle sizes and use the information to describe the flow regimes.

To quantitatively study the pore size and pore throat distribution, we need to envisage a physically based conceptual model to describe the pore structures of permeable stones. The commonly used model is the so-called capillary model (Pittman, 1992; Rezaee et al., 2012; Schmitt et al., 2013), which approximates the connected pores as many paralleled capillaries. And the capillary forces are generated at the phase interface due to the surface tension

https://doi.org/10.5194/hess-2021-588
Preprint. Discussion started: 30 November 2021

Hydrology and Earth System Sciences
Discussions

between the solid and liquid phases when liquid flows in a capillary. The capillary force is directed toward the concave liquid level, and is shown as (Washburn, 1921):

$$P_c = \frac{2\sigma \cos\theta}{r} \tag{3-1}$$

where P_c is the capillary force, σ is the solid-liquid interfacial tension, θ is the wet angle between the liquid and the solid surface, and r is the radius of curvature in capillary.

Since mercury is a nonwetting phase to solids, so to get mercury into the pores of the permeable stone, an external force (or displacement pressure) must be applied to overcome the capillary force. When a greater pressure is applied, mercury can enter smaller pores. When a certain pressure is applied, the injection pressure is equivalent to the capillary pressure in the corresponding pore. Then we can calculate the corresponding capillary radius according to Eq. (3-1), and the volume of mercury injected is the pore volume.

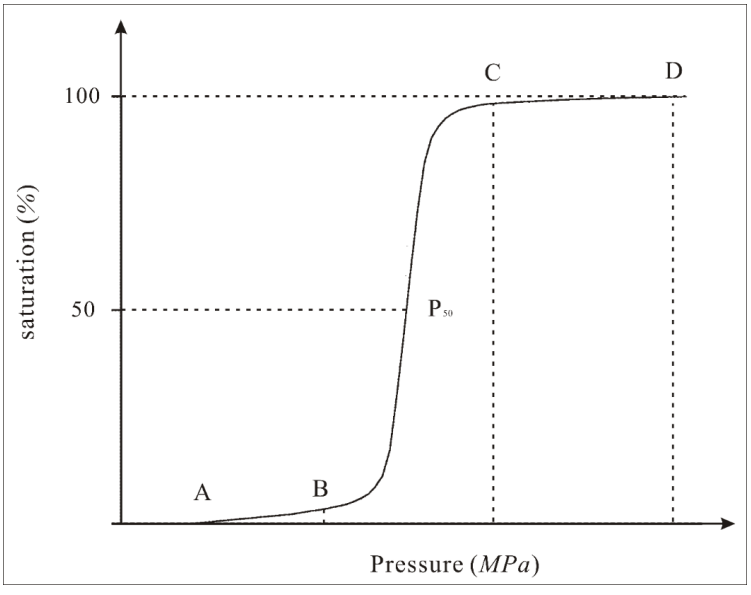

Fig. 6 Schematic diagram of pressure changes with saturation: the initial stage (A-B), the intermediate mercury entry stage (B-C), and the end stage (C-D).

https://doi.org/10.5194/hess-2021-588
Preprint. Discussion started: 30 November 2021


Hydrology and Earth System Sciences
Discussions

By continuously increasing the injection pressure, one can obtain the curve of injection pressure and the volume of injected mercury, from which one can also obtain the pore-throat distribution curve and capillary pressure curve. According to the amount of mercury injected at different injection pressures, the relation between the injection pressure and the injection saturation is shown in Fig. 6.

Fig. 6 shows that the mercury injection curve can be divided into three stages. Firstly, during the initial stage (A-B) which has a very mild slope, the intake pressure is very small and the intake saturation is also very low. With the increasing of the injection pressure, the intake saturation slowly increases. Secondly, during the intermediate mercury entry stage (B-C) which has a steep slope, a small pressure change will lead to a significant saturation change. This means that the pores are relatively uniform and the differences in pore sizes are small. Hence, we can use the pressure ratios of B and C (P_C/P_B) to reflect the inhomogeneity of the pore size in the porous media. Besides, when the saturation reaches 50%, the corresponding pressure value (P_{50}) reflects the characteristics of the mean pore size, and a larger P_{50} leads to a larger mean pore size. Finally, during the end stage (C-D) which has a very mild slope as well, the amount of mercury will not increase considerably when the injection pressure increases. This indicates that nearly all the pores are essentially filled with mercury, and the mercury injection experiment is completed. After completing the mercury injection experiments, we have obtained the mercury injection curves of four permeable stones with different particle sizes, as shown in Fig. 7.

We can make a number of interesting observations based on Fig. 7. Firstly, the pressure at the starting point (when the saturation begins to increase), denoted as P_A, increases as the mean particle size decreases. This means that the maximum pore size in permeable stone decreases with the decrease of the mean particle sizes. Secondly, the mercury injection curves of four permeable stones all include steep intermediate stages, indicating that the pore size

https://doi.org/10.5194/hess-2021-588
Preprint. Discussion started: 30 November 2021

Hydrology and Earth System Sciences
Discussions

distributions are all relatively uniform. And the corresponding pressure values at points B and C increase as the mean particle sizes decreases. Moreover, the pressure ratios corresponding to points B and C (P_C/P_B) also decrease with the decrease of particle sizes, suggesting even more uniform pore size distributions with decreasing particle sizes. Thirdly, the intermediate mercury entry stages gradually shift to the right with the decrease of particle sizes. When the saturation reaches 50%, the corresponding pressure (the median pressure) decreases with the increase of the mean particle sizes. Fourthly, the mercury injection curves of these four permeable stones with different particle sizes all approach 100% saturation with very mild slopes, indicating that there are few small pores in the permeable stones. We have extracted the key pressure characteristic values of mercury injection experiment of Fig. 7, and listed the results in Table 1.

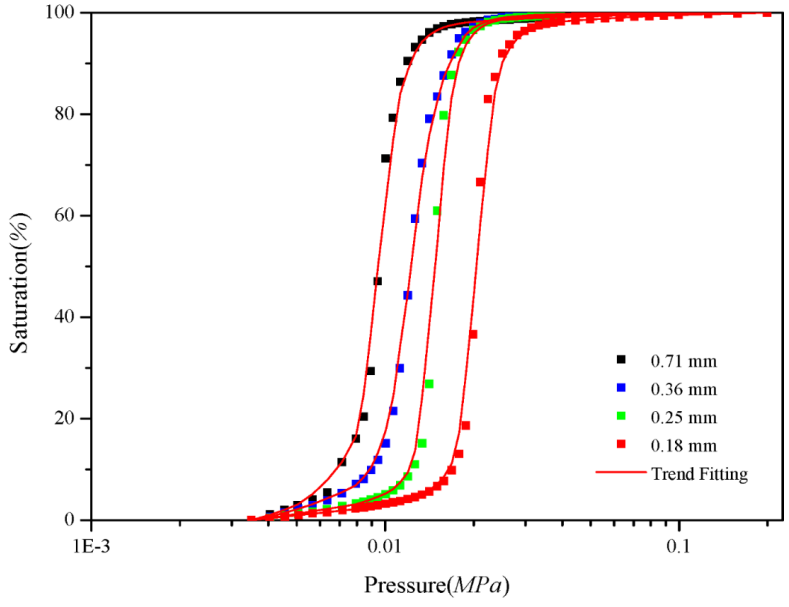

Fig. 7 Variation of pressure with saturation of four permeable stones with different particle sizes.

https://doi.org/10.5194/hess-2021-588
Preprint. Discussion started: 30 November 2021

Hydrology and Earth System Sciences
Discussions
Open Access
EGU

328 Table 1. Pressure characteristic values of four permeable stones with different particle sizes.

Mesh size	$P_A(MPa)$	$P_B(MPa)$	$P_C(MPa)$	$P_{50}(MPa)$	P_C/P_B
24	0.0041	0.0064	0.0133	0.0094	2.0987
46	0.0045	0.0071	0.0188	0.0119	2.6374
60	0.0051	0.0112	0.0211	0.0150	1.8764
80	0.0057	0.0158	0.0281	0.0211	1.7758

329 To observe the pore size distributions of the four permeable stones with different particle
330 sizes in more details, we can calculate the percentages of different pore sizes in permeable
331 stones according to the mercury injection curves, as shown in Figs. 8-11.

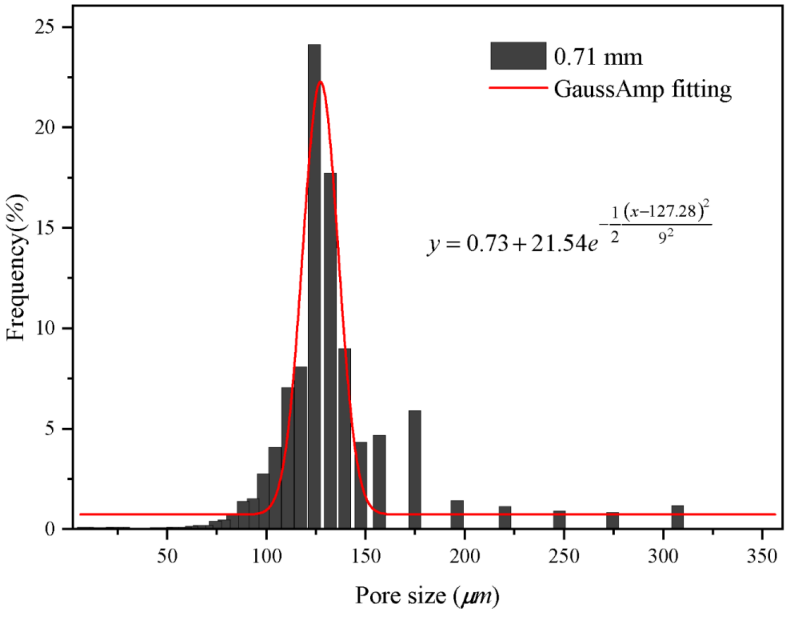

332

333 Fig. 8 Histogram of pore size distribution of permeable stone with diameter of 0.71 mm.

334

https://doi.org/10.5194/hess-2021-588
Preprint. Discussion started: 30 November 2021

Hydrology and Earth System Sciences
Discussions

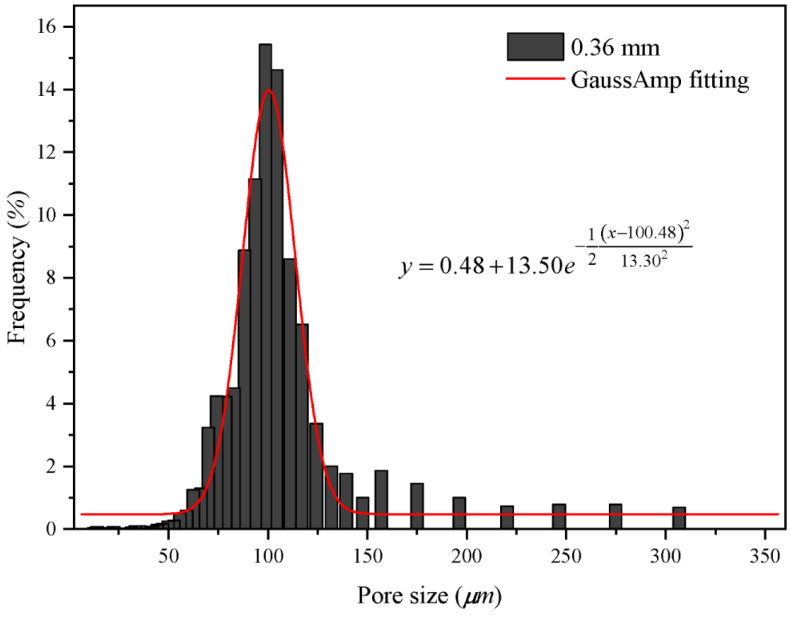

335

336 Fig. 9 Histogram of pore size distribution of permeable stone with diameter of 0.36 mm.

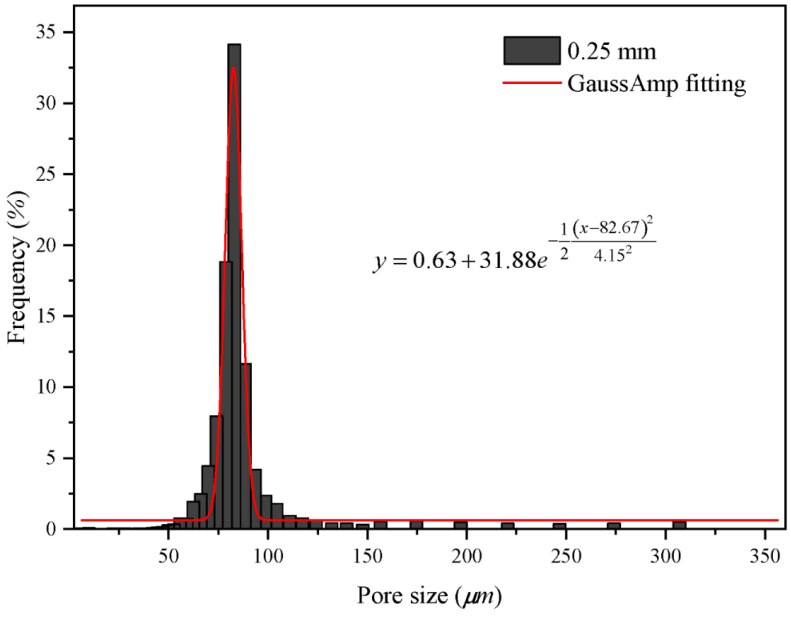

337

338 Fig. 10 Histogram of pore size distribution of permeable stone with diameter of 0.25 mm.

339

https://doi.org/10.5194/hess-2021-588
Preprint. Discussion started: 30 November 2021

Hydrology and Earth System Sciences
Discussions

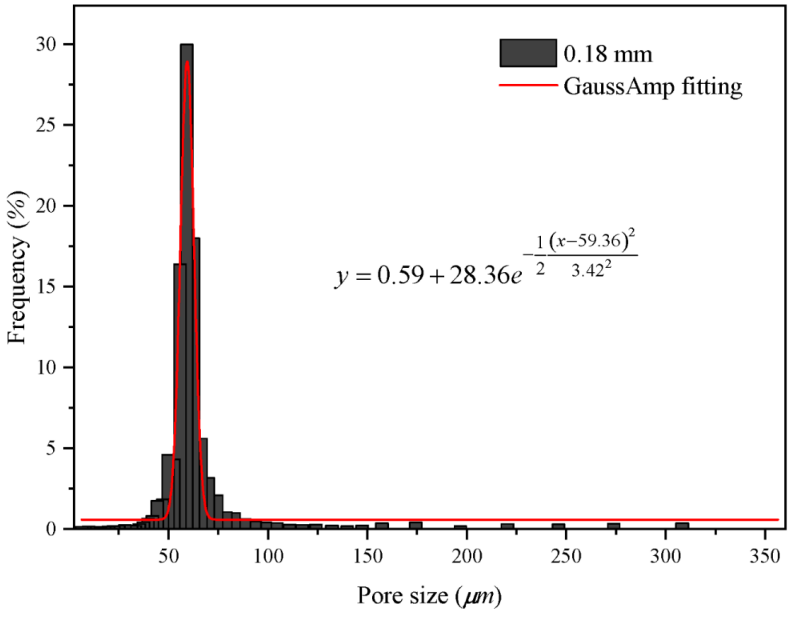

340

341 Fig. 11 Histogram of pore size distribution of permeable stone with diameter of 0.18 mm.

342 From Fig. 8 to Fig. 11 we can find that the pore sizes of the four permeable stones are
343 uniform and fall within narrow ranges. The pore size distributions of four different particle
344 sizes show a skewed normal distribution. Besides, the pore maximum proportion (the peak of
345 the curve, see Figs. 8-11) of permeable stones with different particle sizes are different, which
346 are 124 μm, 99 μm, 83 μm and 59 μm, respectively. The Gaussian function is widely used to
347 characterize the pore system and classify the petrophysical rock (Harlan et al., 1995; Jeon et
348 al., 2014; Xu and Torres-Verdín, 2013), and the general form of the Gauss function is shown
349 below:

$$y = y_0 + He^{-\frac{(x-x_c)^2}{2w^2}} \quad (3\text{-}2)$$

350 where H is the height of the peak of the mercury injection curve, x_c is the abscissa
351 corresponding to the peak of the curve (the pore size), w is the standard variance, which
352 represents the width of the curve. To characterize the distribution of pore structure of four

https://doi.org/10.5194/hess-2021-588
Preprint. Discussion started: 30 November 2021


Hydrology and Earth System Sciences
Discussions

different permeable stones, we best-fit the Gaussian curve of the pore distribution of four permeable stones with different particle sizes, and the best-fitted parameters are shown in Table 2. We can make several interesting observations from Table 2. Firstly, the expected value (x_c) decreases with decreasing particle sizes of permeable stone, and the x_c values of different permeable stones are almost the same. Secondly, the standard variance (w) corresponding to the permeable stone of 0.18 mm is the smallest, indicating that the pore size distribution is more concentrated (or relatively homogeneous). For comparison, the pore size distribution of 0.36 mm permeable stone is the widest with the greatest variance. Finally, different values of H represent different proportions of pore sizes, among which the highest proportion can reach 34.04%. It will be desirable to establish a correlation between the parameters used in the pore-size distribution of Eq. (3-2) with the two Forchheimer coefficients A and B. This objective may be achieved using high-resolution pore-scale fluid mechanics simulations, which are out of the scope of this study. Further research is needed to address this issue in the future.

Table 2. Gaussian function characteristic values of four permeable stones with different particle sizes.

Mesh size	particle size (mm)	y_0	H	x_c	w
24	0.71	0.73	21.54	127.28	9.00
46	0.36	0.48	13.49	100.48	13.30
60	0.25	0.63	31.88	82.67	4.15
80	0.18	0.59	28.36	59.36	3.42

https://doi.org/10.5194/hess-2021-588
Preprint. Discussion started: 30 November 2021

Hydrology and Earth System Sciences
Discussions
Open Access
EGU

370 The pore size distributions fall within ever narrower ranges with mesh sizes become
371 larger. Moreover, the cumulative percentage frequency curves of the pore size distributions
372 with different particle sizes are exhibited in Fig. 12 and the results are shown in Table 3.

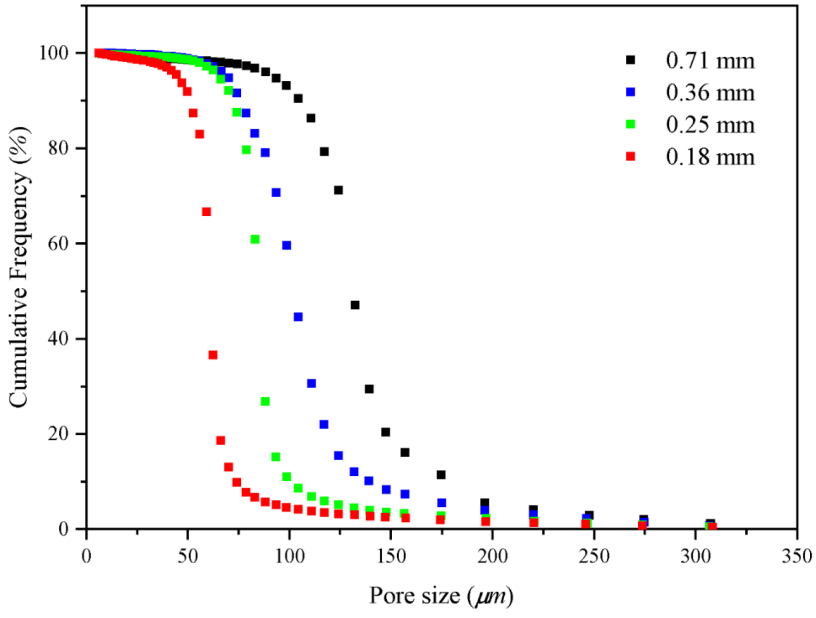

373

374 Fig. 12. The cumulative frequency curve of pore size distribution.

375 Fig. 12 shows that R_{50} (the pore size corresponding to the median pressure P_{50}) increases
376 with the increase of permeable stone particle size, and the mean pore diameter (R_m) also
377 increases. In general, the pore size corresponding to the median pressure (denoted as R_{50})
378 may be slightly different than the mean pore diameter (R_m) which has been defined in
379 different ways by various investigators when analyzing the pore size distributions (Hea and
380 Zhangb, 2015; Zhen-Hua et al., 2007; Zhihong et al., 2000). As R_{50} is easily identifiable in
381 the mercury injection experiments, it is used in this study as a representative of the mean pore
382 diameter (R_m) of the permeable stone. Besides, the seepage law of permeable stone is closely
383 related to the pore size, and the smaller average pore size will result in a larger hydraulic
384 gradient under the condition of the same specific discharge (see Fig. 4). The pore size

https://doi.org/10.5194/hess-2021-588
Preprint. Discussion started: 30 November 2021


Hydrology and Earth System Sciences
Discussions

characteristic values with different particle sizes are listed in Table 3. We find that the porosity decreases as the particle size increases while the mean pore diameter increases. And the mean pore size can reflect the influence of particle diameter, sorting degree and arrangement mode of porous medium on seepage parameters.

Table 3. Pore size characteristic values of four permeable stones with different particle sizes.

Mesh size	Mean particle size (*mm*)	Porosity (%)	R_m (μm)	R_{50} (μm)
24	0.71	32.35	131.31	131.34
46	0.36	36.69	102.56	103.42
60	0.25	40.82	84.73	85.09
80	0.18	42.88	60.97	61.12

Note: R_m is the mean pore diameter, R_{50} is the pore diameter corresponding to the median pressure P_{50}.

3.3 Analysis of influencing factors of Forchheimer equation coefficients

3.3.1 Influence of particle size on equation coefficient

The analysis of non-Darcy coefficient has always been of interest to many researchers working in different disciplines of porous media flow (Moutsopoulos et al., 2009; Sedghi-Asl et al., 2014; Shi et al., 2020). Various studies have suggested expressions for Forchheimer coefficients, Ward (1964) proposed the estimation formula of Forchheimer coefficients *A* and *B* by analyzing the experimental data of 20 different porous media:

$$A=\frac{360}{gd^2} \qquad B=\frac{10.44}{gd} \tag{3-3}$$

https://doi.org/10.5194/hess-2021-588
Preprint. Discussion started: 30 November 2021


Hydrology and Earth System Sciences
Discussions
Open Access
EGU

where d is the particle diameter hereinafter, g is the acceleration due to gravity. Based on the mixed model of parallel capillary tubes, Blick (1966) proposed a new form of Forchheimer coefficients:

$$A=\frac{32}{gnd^2} \qquad B=\frac{C_D}{2gn^2d} \tag{3-4}$$

where n is the porosity of the medium, C_D is an appropriate phenomenological coefficient.

Besides, Ergun (1952) suggested the new expressions by extending the classic Kozeny-Carman model:

$$A=\frac{150(1-n)^2}{gn^3d^2} \qquad B=\frac{1.75(1-n)}{gn^3d} \tag{3-5}$$

Kovács (1981) analyzed 300 data in the range of $10 < Re < 100$, and derived a similar expression for the case of dispersed spherical particles, and the coefficients of Forchheimer are as follows:

$$A=\frac{144(1-n)^2}{gn^3d^2} \qquad B=\frac{2.4(1-n)}{gn^3d} \tag{3-6}$$

Kadlec and Knight (1996) also proposed the following Forchheimer coefficients:

$$A=\frac{255(1-n)^2}{gn^{3.7}d^2} \qquad B=\frac{2(1-n)}{gn^3d} \tag{3-7}$$

Sidiropoulou et al. (2007) focused on the determination of the Forchheimer coefficients for non-Darcian flow in porous media and evaluated the original theoretical equations above and the validity of these equations was checked using existing experimental data. In addition, the Root Mean Square Error (RMSE) was used as a criterion to quantitatively evaluate the

https://doi.org/10.5194/hess-2021-588
Preprint. Discussion started: 30 November 2021


Hydrology and Earth System Sciences
Discussions

coefficients, and the RMSE was defined as $RMES=\sqrt{\frac{\sum_{i=1}^{N}(x_i-y_i)^2}{N}}$, where x_i were the experimental values of Forchheimer coefficients, y_i were the values computed by different equations above, and N was the total number of experimental points (Moutsopoulos et al., 2009). The different forms of Forchheimer coefficients described above are based on different assumptions and simplifications of pore structure. Consequently, these series of coefficients are applicable under specific conditions with different degrees of accuracy.

According to Eq. (1-2), the hydraulic gradient (J) is composed of a viscous force-related component (J_n) and an inertia force-related component (J_r), as below:

$$J_n=Aq=\frac{\alpha\mu}{\rho g}\frac{1}{d^2}q \quad J_r=\frac{\beta}{g}\frac{1}{d}q^2 \tag{3-8}$$

We can see from Eq. (3-8) that the J_n is inversely proportional to the square of the particle size, and the J_r is inversely proportional to the particle size when the specific discharge remains the same. Both J_n and J_r are closely related to specific surface area and sizes of pores. Therefore, the particle size is an important factor affecting the Forchheimer coefficient, Huang et al. (2013) carried out the experimental investigation on water flow in four columns with cubic arrays of acrylic balls in diameter 3 mm, 5 mm, 8 mm and 10 mm, where all the acrylic balls are arranged in regular cubes. Accordingly, the coefficients A and B can be written as follows:

$$A=\frac{\alpha\mu}{\rho g}\frac{1}{d^2} \qquad B=\frac{\beta}{g}\frac{1}{d} \tag{3-9}$$

where α and β are constants related to the shape, sorting, and arrangement of the particles, and the specific derivation process is detailed in the previous study (Huang, 2012). The experimental results showed that the coefficient A was inversely proportional to the particle diameter square (d^2) and coefficient B was inversely proportional to the particle size (d)

https://doi.org/10.5194/hess-2021-588
Preprint. Discussion started: 30 November 2021

Hydrology and Earth System Sciences
Discussions

433 (Huang et al., 2013).

434 The uniform diameter cubic arrangement of porous media mentioned above is a rather
435 ideal medium. The shape and arrangement of particles of natural pore aquifers are usually
436 irregular. Therefore, the above-mentioned linear correlations between A and $1/d^2$, and
437 between B and $1/d$ should be examined specifically. For this purpose, we collect the
438 experimental data of homogeneous porous media, including the previous research results and
439 the results of other scholars. Among them, samples P1-P4 are the permeable stones selected
440 in this study, samples L1-L5 are from previous studies (Li et al., 2017), and the experimental
441 data of samples M1-M4 are from Moutsopoulos et al. (2009). The fitting coefficients are
442 shown in Table 4. Furthermore, we can identify nice correlations between the Forchheimer
443 coefficient A and $1/d^2$ and between the Forchheimer coefficient B and $1/d$, which are shown
444 in Fig. 13 and Fig. 14, respectively.

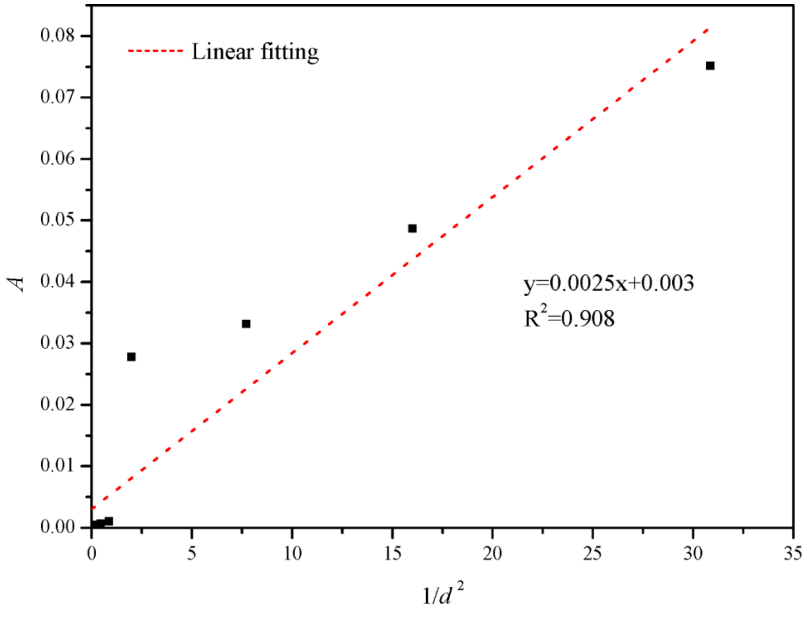

445

446 Fig. 13. Variation of A with $1/d^2$ of different homogeneous particle sizes.

https://doi.org/10.5194/hess-2021-588
Preprint. Discussion started: 30 November 2021

Hydrology and Earth System Sciences
Discussions

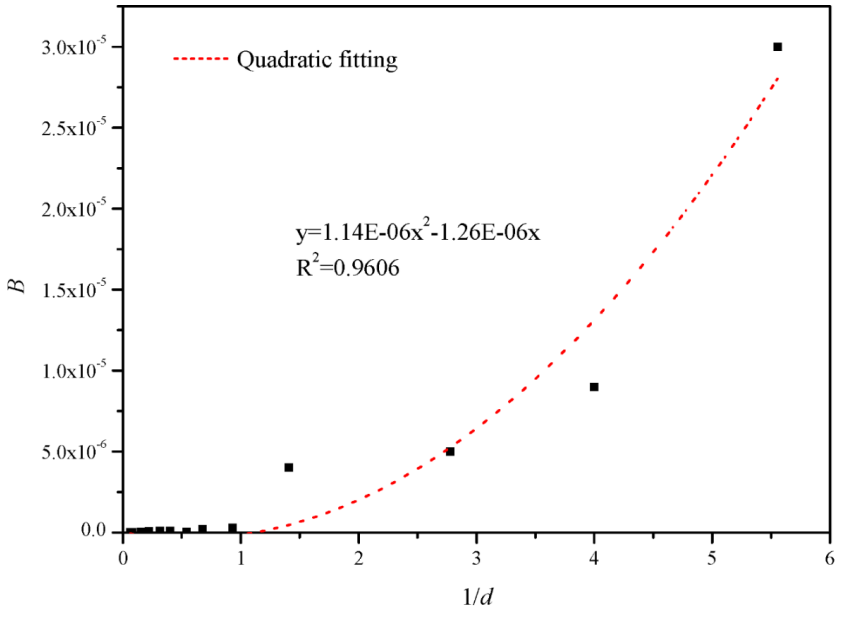

447

448 Fig. 14. Variation of B with $1/d$ of different homogeneous particle sizes.

449 We can see from Fig. 13 that the coefficient A is linearly related to $1/d^2$ and the
450 relationship between coefficient A and is given as $A = 0.0025\left(1/d^2\right) + 0.003$. And the
451 relationship between coefficient B and $1/d$ is completely different from the linear correlation
452 as reported before. Fig. 14 shows that the coefficient B is quadratic related to $1/d$ and the
453 relationship between coefficient B and $1/d$ is given as $B = 1.14\text{E-}06\left(1/d\right)^2 - 1.26\text{E-}06\left(1/d\right)$.
454 That is to say, the relationship between coefficient A and $1/d^2$ is consistent with the law of
455 simple cubic arrangement porous media, but the relationship between coefficient B and $1/d$ is
456 not consistent with the law of simple cubic arrangement porous media. The structure of
457 porous medium arranged in cubes is different from the permeable stone. The porosity of the
458 porous media with spheres arranged in cubic is close to 0.48, independent of the diameter of
459 spheres. While the particle shape, arrangement and tightness of permeable stone are different,
460 and the porosity of permeable stone with different particle size is also different (see Table 3).

https://doi.org/10.5194/hess-2021-588
Preprint. Discussion started: 30 November 2021


Hydrology and Earth System Sciences
Discussions

461 Table 4. Experimental fitting coefficient of different homogeneous particle sizes.

Sample	Particle size (mm)	Fitting equation	A	B	The correlation
P1	0.18	$y=0.0751x+3E-05x^2$	0.0751	3E-05	0.9995
P2	0.25	$y=0.0487x+9E-06x^2$	0.0487	9E-06	0.9998
P3	0.36	$y=0.0331x+5E-06x^2$	0.0331	5E-06	1
P4	0.71	$y=0.0278x+4E-06x^2$	0.0278	4E-06	0.9995
L1	1.075	$y=0.001x+3E-07x^2$	0.001	3E-07	0.9999
L2	1.475	$y=0.0007x+2E-07x^2$	0.0007	2E-07	0.9998
L3	1.85	$y=0.0005x+5E-08x^2$	0.0005	5E-08	0.9998
L4	2.5	$y=0.0005x+9E-08x^2$	0.0005	9E-08	0.9997
L5	3.17	$y=0.0004x+1E-07x^2$	0.0004	1E-07	0.9998
M1	4.5	$y=3E-05x+7E-08x^2$	3E-05	7E-08	0.9913
M2	6.39	$y=3E-05x+3E-08x^2$	3E-05	3E-08	0.9984
M3	12.84	$y=1E-05x+2E-08x^2$	1E-05	2E-08	0.9977
M4	16	$y=1E-05x+2E-08x^2$	1E-05	2E-08	0.998

462 **3.3.2 Influence of porosity on equation coefficient**

463 In above sections, we have analyzed the influence of particle sizes on seepage
464 coefficient. Furthermore, the pore size and pore specific surface area are also related to the
465 arrangement and sorting degree of particles, that is, to the porosity of porous media. To
466 explore the effect of sorting degree on seepage coefficient, we draw a schematic diagram of

https://doi.org/10.5194/hess-2021-588
Preprint. Discussion started: 30 November 2021

Hydrology and Earth System Sciences
Discussions
Open Access
EGU

different sorting degree of particles, as shown in Fig. 15. The degree of particle sorting is one of the important factors affecting the pore size. In porous media with a poor sorting degree, the pore size is usually determined by the diameter of the smallest particle. We can see from Fig. 15 that the pores between the larger particles are filled by smaller particles, resulting in even smaller pores. In addition, the poorer sorting degree of particles leads to the larger pore specific surface area and stronger viscous force of flow, which can lead to a larger coefficient *A*.

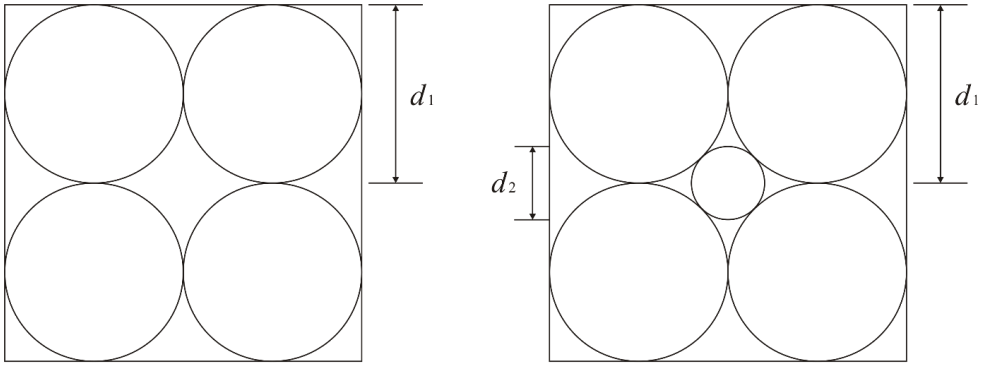

Fig. 15. The schematic diagram of particle sorting degree in different types.

Furthermore, we have also provided the schematic diagrams of spherical particles with equal size in two simple arrangements, namely cube arrangement and hexahedron arrangement, as shown in Fig. 16. And the cube arrangement is the less compact arrangement with a pore diameter of 0.414*d*, while the hexahedron arrangement is the more compact arrangement with a pore diameter of 0.155*d*. The characteristic value of pore structure in different arrangement with the same particle size are shown in Table 5. We can see that different arrangement modes will substantially affect the pore specific surface area and pore size of porous media. The more compactly packed particles lead to the larger pore specific surface area and stronger viscous force. Meanwhile, the smaller pore diameter is associated

https://doi.org/10.5194/hess-2021-588
Preprint. Discussion started: 30 November 2021

485 with stronger effect of viscous force and inertia force. In summary, the better sorting degree
486 of particles leads to the weaker viscous and inertial forces, then the coefficients *A* and *B* will
487 be smaller. As the better sorting degree and the less compact (or looser) arrangement particles
488 mean the larger porosity, so we can conclude that the larger porosity leads to the smaller
489 coefficients *A* and *B* under the condition of the same particle size.

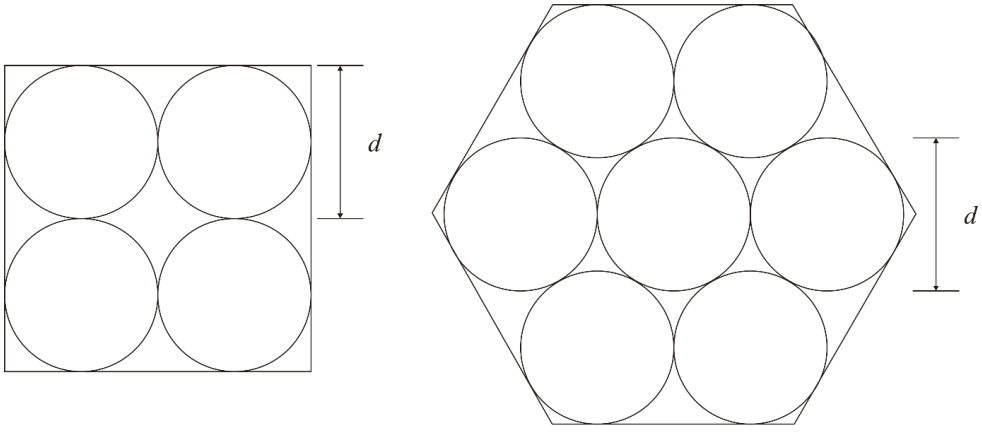

490 （a） （b）

491 Fig. 16. The schematic diagram of particle arrangement in different types.

492 Table 5. Characteristic value of pore structure in different arrangement with the same particle
493 size.

Arrangement mode	Side length	Porosity (%)	Specific surface area
Cube	2*d*	47.60	3.142
Hexahedron	1.577*d*	43.30	3.402

494 However, the structure of natural porous media is much more complex and
495 heterogeneous than what has been shown in Figure 16, so it is difficult to quantitatively
496 describe the effect of sorting degree and arrangement on seepage law.

https://doi.org/10.5194/hess-2021-588
Preprint. Discussion started: 30 November 2021

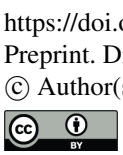

Hydrology and Earth System Sciences
Discussions

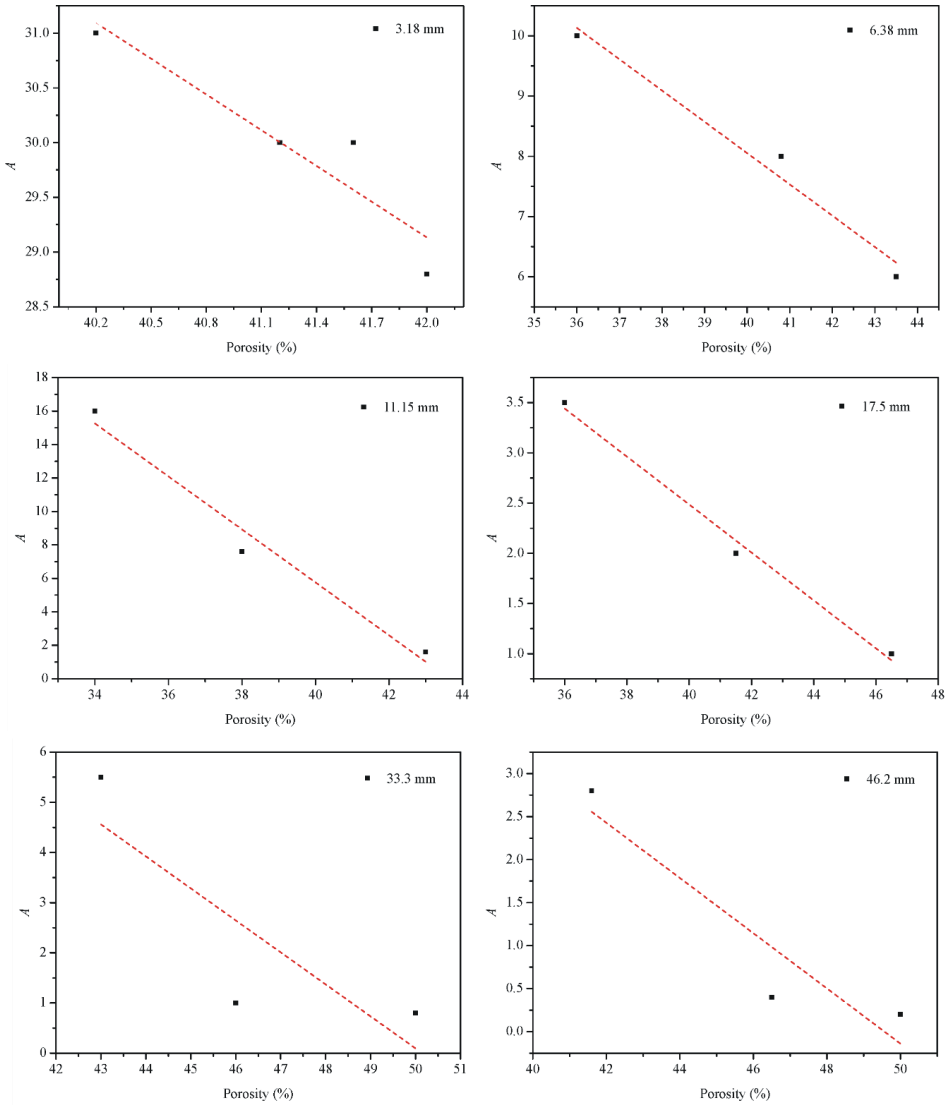

497

498 Fig. 17. Variation of *A* with *n* of six gravels with different particle sizes.

499 In view of this, we can use a macro parameter porosity (*n*) to reveal the effect of sorting
500 degree and arrangement on seepage coefficient. In order to verify the correctness of the above
501 analysis results, we selected the seepage experiment results of Niranjan (1973) for further
502 validation. Niranjan (1973) chose gravel of the same size but different porosity and carried
503 out seepage experiments. We selected the experimental results of six different particle sizes

https://doi.org/10.5194/hess-2021-588
Preprint. Discussion started: 30 November 2021

Hydrology and Earth System Sciences
Discussions
Open Access
EGU

504 with 3.18 mm, 6.38 mm, 11.15 mm, 17.5 mm, 33.3 mm and 46.2 mm from Niranjan (1973),
505 and drew the relationship between coefficient *A* and *B* and porosity respectively, as shown in
506 Fig. 17 and Fig. 18. We can see that the coefficients *A* and *B* of the six groups of experimental
507 data of Niranjan (1973) decrease with the increase of porosity, which is consistent with our
508 theoretical analysis of this investigation.

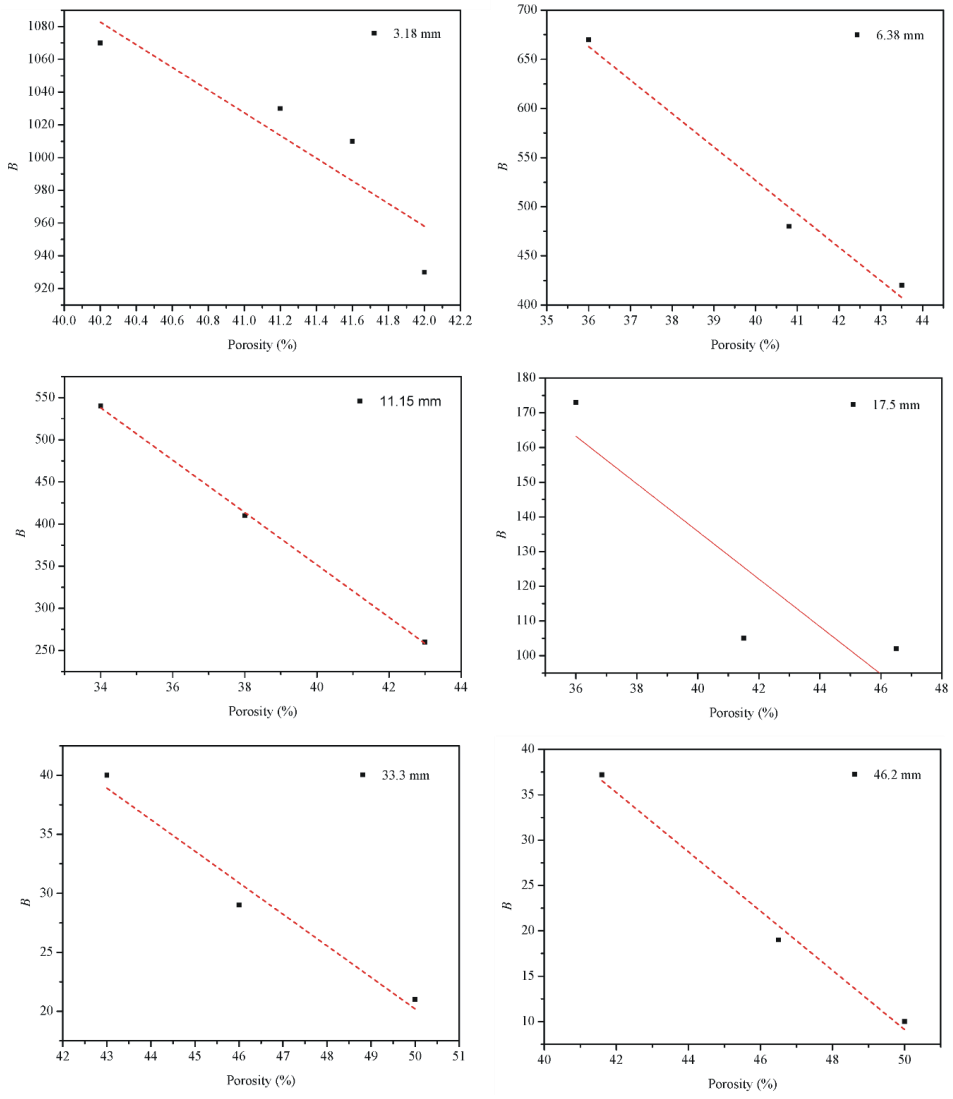

509

510 Fig. 18. Variation of *B* with *n* of six gravels with different particle sizes.

https://doi.org/10.5194/hess-2021-588
Preprint. Discussion started: 30 November 2021


Hydrology and Earth System Sciences
Discussions

4. Summary and conclusions

This study presents experimental results of Forchheimer flow in four different permeable stones with different mesh sizes, including 24 mesh size (0.71 mm), 46 mesh size (0.36 mm), 60 mesh size (0.25 mm), 80 mesh size (0.18 mm). The effects of mean pore size and pore size distribution on the transition of flow regimes (from pre-Darcian to post-Darcian) are discussed. In addition, the mercury injection experiment is proposed to investigate the pore distribution of the permeable stones. In addition, the Forchheimer coefficients are specifically discussed. The main conclusions can be summarized as follows:

1) The relationships between specific discharge (q) and the “pseudo” hydraulic conductivity (K) (which is computed as a ratio of q and hydraulic gradient, J) of permeable stones show that deviation from Darcian flow regime is clearly visible. In addition, the critical specific discharge corresponding to the transition of flow regimes (from pre-Darcian to post-Darcian) increases with the increase of mean particle size.

2) When the specific discharge is small, only a small fraction of the water flowing through the pores. The rest of the water adheres to the surface of the solid particles (immobile), partially blocking the flow pathways. As the specific discharge increases, more water becomes mobile and participates in flow. Hence, the "pseudo" hydraulic conductivity increases with the increase of specific discharge. When the specific discharge increases to the critical specific discharge (q_c), the "pseudo" hydraulic conductivity is maximized, and then it begins to decrease as the specific discharge continues to increase.

3) The mercury injection experiment results show that the mercury injection curve can be divided into three segments. The beginning and end segments of the mercury injection curve of the four permeable stones with different particle sizes are very gentle, while the main (or intermediate) mercury injection curve is steep, indicating that the pore size distribution falls within a narrow range, and the proportions of large pores and small pores are relatively small.

https://doi.org/10.5194/hess-2021-588
Preprint. Discussion started: 30 November 2021


Hydrology and Earth System Sciences
Discussions

4) The porosity decreases as the mean particle size of permeable stone increases while the mean pore diameter increases. And the porosity can reflect the influence of particle diameter, sorting degree and arrangement mode of porous medium on seepage parameters. The larger porosity leads to the smaller coefficients *A* and *B* under the condition of the same particle size. 5) The coefficient *A* is linearly related to $1/d^2$ and the relationship between coefficient *A* and $1/d^2$ is given as $A = 0.0025\left(1/d^2\right) + 0.003$. The coefficient *B* is not linearly related to $1/d$, instead it is quadratic related to $1/d$ as $B = 1.14\text{E-}06\left(1/d\right)^2 - 1.26\text{E-}06\left(1/d\right)$. The particle shape and arrangement of permeable stone have imposed great influences on the seepage parameters.

Notation

q	The specific discharge, m/d.
K	The Hydraulic conductivity, m/d.
J	The dimensionless parameter defined as hydraulic gradient.
A	The Forchheimer equation coefficient (viscous force item), sm^{-1}.
B	The Forchheimer equation coefficient (Inertia force item), s^2m^{-2}.
P_c	The capillary force, *Pa*.
P_{50}	The corresponding pressure value when the saturation reaches 50%, *MPa*.
P_A, P_B, P_C	The pressure corresponding to different stages on mercury injection curve, *MPa*.
σ	The solid-liquid interfacial tension.
θ	The wet angle between the liquid and the solid surface.
r	The radius of curvature in capillary, mm.
d	The particle size, mm.

https://doi.org/10.5194/hess-2021-588
Preprint. Discussion started: 30 November 2021


Hydrology and Earth System Sciences
Discussions

558	d_{50}	The mean particle sizes (50% by weight), mm.
559	R_m	The mean pore diameter, μm.
560	R_{50}	The pore diameter corresponding to the median pressure P_{50}, μm.
561	H	The height of the peak of the mercury injection curve.
562	x_c	The abscissa corresponding to the peak of the curve (the pore size).
563	w	The standard variance.
564	n	The porosity.
565	J_n	The viscous force-related component.
566	J_r	The inertia force-related component.

567 **Authors contributions**

568 Zhongxia Li: Experiment, Writing original draft. Junwei Wan: Methodology,
569 Conceptualization. Tao Xiong: Data curation, Investigation, Experiment. Hongbin Zhan:
570 Methodology, Writing, Review & Editing. Linqing He: Experiment, Methodology. Kun
571 Huang: Funding acquisition, Investigation

572 **Competing interests**

573 The authors declare that they have no conflict of interest.

574 **Acknowledgements**

575 This study was supported by the National Natural Science Foundation of China (Grant
576 Nos. 41402204), the National Key Research and Development Program of China
577 (No. 2018YFC0604202) and the Fundamental Research Funds for National Universities,
578 China University of Geosciences (Wuhan). Thank Zhongzhi Shen of China University of
579 Geosciences for his great help in developing the experimental set up. And the authors want to

https://doi.org/10.5194/hess-2021-588
Preprint. Discussion started: 30 November 2021

express their sincere appreciation of the constructive comments made by the three anonymous reviewers and Associate Editor for improving the quality of the manuscript.

References

Anovitz, L. M. and Cole, D. R.: Characterization and Analysis of Porosity and Pore Structures, Reviews in Mineralogy and Geochemistry, 80, 61-164, https://doi.org/10.2138/rmg.2015.80.04, 2015.

Bear, J.: Dynamics of Fluids in Porous Media, American Elsevier Pub. Co., New York, N.Y., and Amsterdam, 1972.

Beavers, G. S., Sparrow, E., and Rodenz, D. E.: Influence of Bed Size on the Flow Characteristics and Porosity of Randomly Packed Beds of Spheres, Journal of Applied Mechanics, 40, 655-660, https://doi.org/10.1115/1.3423067, 1972.

Blick, E.: Capillary-Orifice Model for High-Speed Flow through Porous Media, Industrial Engineering Chemistry Process Design Development, 5, 90-94, https://doi.org/10.1021/i260017a019, 1966.

Bu, S., Yang, J., Dong, Q., and Wang, Q.: Experimental study of transition flow in packed beds of spheres with different particle sizes based on electrochemical microelectrodes measurement, Applied Thermal Engineering, 73, 1525-1532, 2014.

Darcy, H.: Recherches expérimentales relatives au mouvement de l'eau dans les tuyaux, Impr. Impériale, Paris, France, 1857.

Dudgeon, C. R.: An experimental study of the flow of water through coarse granular media, La Houille Blanche, 785-801, https://doi.org/10.1051/lhb/1966049, 1966.

Dybbs, A. and Edwards, R.: A new look at porous media fluid mechanics—Darcy to turbulent, in: Fundamentals of transport phenomena in porous media, Springer, 199-256, 1984.

Ergun, S.: Fluid flow through packed columns, Chemical Engineering Progress, 89-94, https://doi.org/10.1016/0009-2509(53)80048-5, 1952.

Fancher, G. H. and Lewis, J. A.: Flow of simple fluids through porous materials, Industrial & Engineering Chemistry, 25, 1139-1147, https://doi.org/10.1021/ie50286a020, 1933.

Fetter, C. W.: Applied Hydrogeology:International Edition, Prentice Hall, Pearson, Engelwood Cliffs, 2001.

Forchheimer, P.: Wasserbewegung durch boden, Z. Ver. Deutsch, Ing., 45, 1728-1782, 1901.

Geertsma, J.: Estimating the Coefficient of Inertial Resistance in Fluid Flow Through Porous Media, Society of Petroleum Engineers Journal, 14, 445-450, https://doi.org/10.2118/4706-PA, 1974.

Hall, P. L., Mildner, D., and Borst, R. L.: Small-angle scattering studies of the pore spaces of shaly rocks, Journal of Geophysical Research Atmospheres, 91, 2183-2192, https://doi.org/10.1029/JB091iB02p02183, 1986.

Harlan, J., Picot, D., Loll, P., and Garavito, R.: Calibration of size-exclusion chromatography: use of a double Gaussian distribution function to describe pore sizes, Analytical biochemistry, 224, 557-563, https://doi.org/10.1006/abio.1995.1087, 1995.

Hea, X. and Zhangb, Z.: Microscopic Pore Structural Characteristics in Coal Particles, International Conference on Material, Guangzhou, China,

Huang, K.: Exploration of the basic seepage equation in porous media, Ph.D., dissertation, China University of Geosciences, Wuhan, 2012.

Huang, K., Wan, J., Chen, C., Linqing, H., Mei, W., and Zhang, M.: Experimental investigation on water flow in

619 cubic arrays of spheres, Journal of Hydrology, 492, 61-68, https://doi.org/10.1016/j.jhydrol.2013.03.039, 2013.
620 Izbash, S.: O Filtracii V Kropnozernstom Materiale, Leningrad, USSR, 1931.
621 Jeon, H., Cho, H., Kim, J., and Sung, B.: Non-Gaussian rotational diffusion in heterogeneous media, Physical
622 Review E Statistical Nonlinear & Soft Matter Physics, 90, 042105, https://doi.org/10.1103/PhysRevE.90.042105,
623 2014.
624 Kadlec, R. H. and Knight, R. L.: Treatment Wetlands, Lewis Pub, Boca Raton, 1996.
625 Kate, J. M. and Gokhale, C. S.: A simple method to estimate complete pore size distribution of rocks,
626 Engineering Geology, 84, 48-69, https://doi.org/10.1016/j.enggeo.2005.11.009, 2006.
627 Koch, D. and Ladd, A.: Moderate Reynolds number flows through periodic and random arrays of aligned
628 cylinders, Journal of Fluid Mechanics, 349, 31-66, https://doi.org/10.1017/S002211209700671X, 1996.
629 Kovács, G.: Seepage Hydraulics, Development in Water Sciences. Elsevier: New York, 1981.
630 Latifi, M., Midoux, N., Storck, A., and Gence, J.: The use of micro-electrodes in the study of the flow regimes in
631 a packed bed reactor with single phase liquid flow, Chemical engineering science, 44, 2501-2508, 1989.
632 Li, Z., Wan, J., Huang, K., Chang, W., and He, Y.: Effects of particle diameter on flow characteristics in sand
633 columns, International Journal of Heat & Mass Transfer, 104, 533-536,
634 https://doi.org/10.1016/j.ijheatmasstransfer.2016.08.085, 2017.
635 Li, Z., Wan, J., Zhan, H., Cheng, X., Chang, W., and Huang, K.: Particle size distribution on Forchheimer flow
636 and transition of flow regimes in porous media, Journal of Hydrology, 574, 1-11,
637 https://doi.org/10.1016/j.jhydrol.2019.04.026, 2019.
638 Lindquist, E.: On the flow of water through porous soil, Premier Congres des grands barrages (Stockholm), 81-
639 101,
640 Lindquist, W. B., Venkatarangan, A., Dunsmuir, J., and Wong, T. F.: Pore and throat size distributions measured
641 from synchrotron X-ray tomographic images of Fontainebleau sandstones, Journal of Geophysical Research
642 Solid Earth, 105, 21509-21527, https://doi.org/10.1029/2000JB900208, 2000.
643 Maalal, O., Prat, M., Peinador, R., and Lasseux, D.: Determination of the throat size distribution of a porous
644 medium as an inverse optimization problem combining pore network modeling and genetic and hill climbing
645 algorithms, Physical Review E, 103, 023303, https://doi.org/10.1103/PhysRevE.103.023303, 2021.
646 Moutsopoulos, K. N., Papaspyros, I. N., and Tsihrintzis, V. A.: Experimental investigation of inertial flow
647 processes in porous media, Journal of hydrology, 374, 242-254, https://doi.org/10.1016/j.jhydrol.2009.06.015,
648 2009.
649 Niranjan, H.: Non-Darcy flow through porous media, M.S., dissertation, ITT, Kanpur, India, 1973.
650 Panfilov, M. and Fourar, M.: Physical splitting of nonlinear effects in high-velocity stable flow through porous
651 media, Advances in Water Resources, 29, 30-41, https://doi.org/10.1016/j.advwatres.2005.05.002, 2006.
652 Pittman, E. D.: Relationship of porosity and permeability to various parameters derived from mercury injection-
653 capillary pressure curves for sandstone (1), AAPG bulletin, 76, 191-198, https://doi.org/10.1306/BDFF87A4-
654 1718-11D7-8645000102C1865D, 1992.
655 Rezaee, R., Saeedi, A., and Clennell, B.: Tight gas sands permeability estimation from mercury injection
656 capillary pressure and nuclear magnetic resonance data, Journal of Petroleum Science and Engineering, 88, 92-
657 99, https://doi.org/10.1016/j.petrol.2011.12.014, 2012.
658 Rijfkogel, L. S., Ghanbarian, B., Hu, Q., and Liu, H. H.: Clarifying pore diameter, pore width, and their
659 relationship through pressure measurements: A critical study, Marine and Petroleum Geology, 107, 142-148,
660 https://doi.org/10.1016/j.marpetgeo.2019.05.019, 2019.

https://doi.org/10.5194/hess-2021-588
Preprint. Discussion started: 30 November 2021

Hydrology and Earth System Sciences
Discussions

661 Scheidegger, A.: The physics of flow through porous media,
662 Scheidegger, A. E.: On the stability of displacement fronts in porous media: a disscussion of the muskat-
663 aronofsky model, Canadian Journal of Physics, 38, 153-162, https://doi.org/10.1139/p60-017, 1960.
664 Schmitt, M., Fernandes, C. P., da Cunha Neto, J. A., Wolf, F. G., and dos Santos, V. S.: Characterization of pore
665 systems in seal rocks using nitrogen gas adsorption combined with mercury injection capillary pressure
666 techniques, Marine and Petroleum Geology, 39, 138-149, https://doi.org/10.1016/j.marpetgeo.2012.09.001, 2013.
667 Schneebeli, G.: Experiences sur la limite de validite de la loi de Darcy et l'apparition de la turbulence dans un
668 ecoulemant de filtration, La Huille Blanche, 2, 141-149, https://doi.org/10.1051/lhb/1955030, 1955.
669 Sedghi-Asl, M., Rahimi, H., and Salehi, R.: Non-Darcy Flow of Water Through a Packed Column Test,
670 Transport in Porous Media, 101, 215-227, https://doi.org/10.1007/s11242-013-0240-0, 2014.
671 Seguin, D., Montillet, A., Comiti, J., and Huet, F.: Experimental characterization of flow regimes in various
672 porous media—II: Transition to turbulent regime, Chemical engineering science, 53, 3897-3909, 1998.
673 Shi, W., Yang, T., and Yu, S.: Experimental Investigation on Non-Darcy Flow Behavior of Granular Limestone
674 with Different Porosity, Journal of Hydrologic Engineering, 25, 06020004,
675 https://doi.org/10.1061/(ASCE)HE.1943-5584.0001966, 2020.
676 Sidiropoulou, M. G., Moutsopoulos, K. N., and Tsihrintzis, V.: Determination of Forchheimer equation
677 coefficients a and b, Hydrological Processes, 21, 534-554, https://doi.org/10.1002/hyp.6264, 2007.
678 Skjetne, E., Hansen, A., and Gudmundsson, J.: High-velocity flow in a rough fracture, Journal of Fluid
679 Mechanics, 383, 1-28, https://doi.org/10.1017/S0022112098002444, 1999.
680 Souto, H. P. A. and Moyne, C.: Dispersion in two-dimensional periodic porous media. Part I. Hydrodynamics,
681 Physics of Fluids, 9, 2243-2252, https://doi.org/10.1063/1.869365, 1997.
682 Van Lopik, J. H., Zazai, L., Hartog, N., and Schotting, R.: Nonlinear Flow Behavior in Packed Beds of Natural
683 and Variably Graded Granular Materials, Transport in Porous Media, 131, 957-983,
684 https://doi.org/10.1007/s11242-019-01373-0, 2019.
685 Van Lopik, J. H., Snoeijers, R., van Dooren, T. C. G. W., Raoof, A., and Schotting, R. J.: The Effect of Grain
686 Size Distribution on Nonlinear Flow Behavior in Sandy Porous Media, Transport in Porous Media, 120, 1-30,
687 https://doi.org/10.1007/s11242-017-0903-3, 2017.
688 Ward, J. C.: Turbulent Flow in Porous Media, Journal of Hydraulic Engineering, 90, 1-12,
689 http://dx.doi.org/10.1016/S0301-9322(02)00051-4, 1964.
690 Washburn, E. W.: The Dynamics of Capillary Flow, Physical Review, 17, 273-283,
691 https://doi.org/10.1103/PhysRev.17.273, 1921.
692 Wright, D.: Nonlinear Flow Through Granular Media, Journal of Hydraulic Engineering, 94, 851-872,
693 https://doi.org/10.1061/JYCEAJ.0001858, 1968.
694 Xu, C. and Torres-Verdín, C.: Pore System Characterization and Petrophysical Rock Classification Using a
695 Bimodal Gaussian Density Function, Mathematical Geosciences, 45, 753-771, https://doi.org/10.1007/s11004-
696 013-9473-2, 2013.
697 Yang, B., Yang, T., Xu, Z., Liu, H., Yang, X., and Shi, W.: Impact of Particle-Size Distribution on Flow
698 Properties of a Packed Column, Journal of Hydrologic Engineering, 24, 04018070,
699 https://doi.org/10.1061/(ASCE)HE.1943-5584.0001735, 2019.
700 Zhen-hua, MIN, and, Min, CAO, and, Shu, ZHANG, and, and Xiu-dan: Effect of precursor on the pore structure
701 of carbon foams, New Carbon Materials, 22, 75-79, https://doi.org/10.1016/S1872-5805(07)60009-2, 2007.
702 Zhihong, L. I., Jihong, S., Dong, W. U., Yuhan, S., Liu, Y. I., Wenjun, S., and Baozhong, D.: Determination of

https://doi.org/10.5194/hess-2021-588
Preprint. Discussion started: 30 November 2021

Hydrology and Earth System Sciences
Discussions
Open Access
EGU

703 average pore diameter of SiO2 xerogels by small angle X-ray scattering, ACTA Physica sinica, 49, 1312-1315,
704 https://doi.org/10.3321/j.issn:1000-3290.2000.07.020, 2000.
705 Zhou, H., Fang, Y.-g., Chen, M., Gu, R.-g., and Li, W.: Experimental and analytical study on electro-osmosis in
706 low-permeability soil considering the pore size effect, Geotechnique, 71, 141-152,
707 https://doi.org/10.1680/jgeot.18.p.362, 2019.

708

709

710